

Thermal characterization of anisotropic media in photothermal point, line, and grating configuration

G. Kalogiannakis, D. Van Hemelrijck, S. Longuemart, J. Ravi, A. Okasha, and C. Glorieux

Citation: *Journal of Applied Physics* **100**, 063521 (2006); doi: 10.1063/1.2335381

View online: <http://dx.doi.org/10.1063/1.2335381>

View Table of Contents: <http://scitation.aip.org/content/aip/journal/jap/100/6?ver=pdfcov>

Published by the [AIP Publishing](#)

Articles you may be interested in

[Thermal properties of carbon nanowall layers measured by a pulsed photothermal technique](#)
Appl. Phys. Lett. **102**, 061903 (2013); 10.1063/1.4791686

[Diffusion in inhomogeneous and anisotropic media](#)
J. Chem. Phys. **119**, 5171 (2003); 10.1063/1.1597476

[Floquet wave homogenization of periodic anisotropic media](#)
J. Acoust. Soc. Am. **112**, 38 (2002); 10.1121/1.1488942

[Gaussian beam propagation in anisotropic, inhomogeneous elastic media](#)
AIP Conf. Proc. **615**, 123 (2002); 10.1063/1.1472789

[Systematic study of second harmonic thermal wave detection based on IR radiometry](#)
AIP Conf. Proc. **463**, 50 (1999); 10.1063/1.58124

An advertisement for Asylum Research Cypher AFMs. The background is a dark blue gradient with a film strip on the left side. The text is in white and orange. The main text reads: 'Not all AFMs are created equal', 'Asylum Research Cypher™ AFMs', and 'There's no other AFM like Cypher'. At the bottom, there is a website URL and the Oxford Instruments logo with the tagline 'The Business of Science®'.

Not all AFMs are created equal
Asylum Research Cypher™ AFMs
There's no other AFM like Cypher

www.AsylumResearch.com/NoOtherAFMLikeIt

OXFORD
INSTRUMENTS
The Business of Science®

Thermal characterization of anisotropic media in photothermal point, line, and grating configuration

G. Kalogiannakis^{a)} and D. Van Hemelrijck

Department of Mechanics of Materials and Constructions (MEMC), Vrije Universiteit Brussel, Brussels B1050, Belgium

S. Longuemart

Laboratory of Thermophysics of Condensed Matter (group of UMR CNRS 8024), University of Littoral Cote d'Opale, MREI, 59140 Dunkerque, France

J. Ravi

Centre for Excellence in Lasers and Optoelectronic Science (CELOS), Cochin University of Science and Technology, Kochi, 682 022 Kerala, India

A. Okasha and C. Glorieux

Laboratory of Acoustics and Thermal Physics (ATF), Department of Physics and Astronomy, Katholieke Universiteit Leuven, B3001 Heverlee, Belgium

(Received 5 December 2005; accepted 13 July 2006; published online 27 September 2006)

This article is dedicated to the simulation of heat diffusion in layered anisotropic materials. The three-dimensional heat diffusion equation for layered, anisotropic materials is used to calculate a laser induced dynamic temperature distribution, the so-called thermal-wave field, in composites. In the case of isotropic materials, the thermal-wave distribution is always axisymmetric around the center of the heat source. In multilayered fiber reinforced composites, however, the distribution of the thermal-wave field depends on their characteristic stacking sequence as well as on the geometry and the frequency of the source. Together with undergoing experimental work, these theoretical simulations allow us to compare the feasibility of different spatial excitation geometries, namely, point source, line source, and grating source, to determine the thermal conductivity tensor of composite materials. It is proven that the use of a grating suppresses the ill posedness of the inverse problem and simplifies the procedure used for the determination of the thermal properties. © 2006 American Institute of Physics. [DOI: [10.1063/1.2335381](https://doi.org/10.1063/1.2335381)]

INTRODUCTION

As mentioned in the thorough work on thermal diffusion of Carslaw and Jaeger,¹ the mathematical theory of heat conduction in anisotropic media for the study of crystals was developed by Duhamel in 1832.^{2,3} Later on Stokes⁴ presented a treatment that is essentially the conventional form used by Carslaw and Jaeger in their approach. A complete analytical study was performed by Boussinesq⁵ in 1901 and, from the viewpoint of crystal physics, by Voigt⁶ a few years later.

Conventional approaches using transformation of the space variables were inadequate to provide full analytical solutions for complicated cases of anisotropic solids under various types of heat excitation. Some reports were, however, presented for simple cases in the 60s. Giedt and HornBaker⁷ solved a simple case of a thermally orthotropic plate in the steady state regime and Touryan⁸ assessed the transient temperature field for a thermally orthotropic cylindrical shell. Chao⁹ also presented a simplification of anisotropic heat conduction to the orthotropic case whereas Padovan¹⁰ considered the heat conduction in a thin cylindrical shell of anisotropic media through the solution of an approximately formulated differential equation. Later on, he

presented the exact analytical solution of heat conduction in infinite composite slabs and cylinders in the form of series with discrete eigenvalues in each direction.¹¹ The solution of the same problem was reported by Turkan and Tuna¹² who extended an approximate continuum theory on elasticity to heat conduction.

Chang *et al.*¹³ and Chang¹⁴ did extensive work with the use of Green's functions to transform the heat conduction differential equations for generally anisotropic media both in cartesian and in cylindrical^{15,16} coordinates into integral equations, which they solved by means of numerical methods. They investigated various geometries such as infinite and semi-infinite domains as well as square, circular, and annular disks and they found their results in good agreement with exact solutions wherever possible. Numerical approaches were also applied by other researchers, such as Katayama¹⁷ who employed the finite difference method and found his calculated results in good agreement with experimental data. The same technique was applied later by Petts and Wickramasinghe¹⁸ obtaining similar successful results. Cobble¹⁹ solved also numerically the heat conduction in a wedge by first transforming the partial differential equation into an ordinary differential equation. The direct solution in the integral form has also been applied by several researchers.^{20–22}

In the last decade, a lot of progress has been achieved

^{a)}Author to whom correspondence should be addressed; FAX: +32-(0)26292928; Electronic mail: georgios_kalogiannakis@yahoo.com

both in the theoretical as well as the experimental field of photothermal methods in anisotropic solids and composite materials in particular. Salazar and co-workers^{23–34} have modeled thermal-wave scattering from various subsurface structures including planar inclusions, spheres, and cylinders. They have been able to successfully characterize and experimentally verify with the mirage effect of the anisotropy of unidirectional fiber reinforced composites. Similar results were experimentally obtained by Lauriks *et al.*³⁵ for carbon fiber reinforced composites.

A detailed numerical study in combination with experimental results using infrared imaging with a pulsed heat source was recently conducted by Krapez *et al.*³⁶ Their simulations were subsequently verified experimentally for harmonic thermal waves (lock-in thermography) by Wu *et al.*³⁷ and Karpen *et al.*³⁸ The same group has recently developed a semianalytical model,³⁹ which uses the recursive algorithm of Grosse and Wynands,⁴⁰ to find the solution in the Fourier coordinates. Then, an inverse fast Fourier transform (FFT) transforms the temperature to the Cartesian spatial coordinates allowing a fast numerical simulation of the thermal-wave field at the surface of multilayered composites assumed to have an infinite absorption coefficient. The latter assumption limits the investigation on carbon fiber reinforced composites, as, from the typically used fibers, carbon only has a very high absorption coefficient at the laser wavelength. Still, it was proven in practice that, because of the rather transparent epoxy matrix, the absorption coefficient cannot be considered infinite for carbon composites either. Our model is adapted for a multilayer system that allows different finite absorption coefficients for each layer. Thus, it can accommodate composite materials with fibers other than carbonlike glass or Kevlar and mixtures of them in different layers. It can moreover be used to find the temperature distribution in planes other than the surface. In what follows, simulations and experimental measurements demonstrate the formation of the temperature field at the surface and how it can be used for the determination of the thermal properties as well as the consisting stacking sequence of layers of a composite laminate. The first part of this study is dealing with the theoretical treatment of thermal waves in anisotropic multilayered media and simulations for different stacking sequences. It also describes a method for the determination of thermal properties using grating excitation.

FORMULATION OF 3D ANISOTROPIC HEAT DIFFUSION BY THE TRANSFER FUNCTION FORMALISM

The so-called transfer function formalism⁴¹ was used to solve the heat diffusion equation for multilayered anisotropic solids such as composite laminates [Fig. 1(a)]. In the present study, a periodically modulated laser induced heat source with different spatial geometries is considered. Firstly, the method will be used to illustrate the formation of the thermal-wave field in unidirectional, cross-ply, and quasi-isotropic laminates for different excitation frequencies. Secondly, for the determination of the thermal properties of the composite material, the results of the theoretical method will be fitted to the experimental measurements.

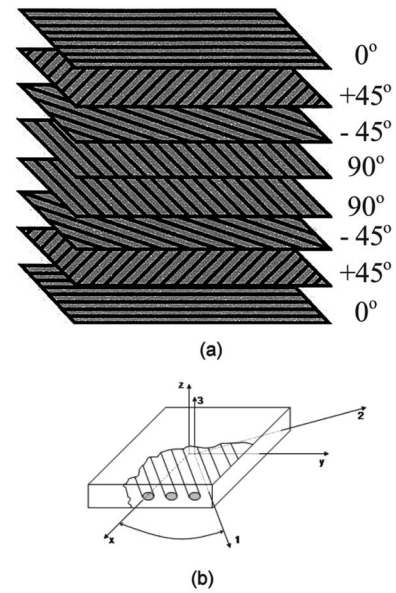


FIG. 1. (a) Fiber reinforced composite laminate and (b) rotation from the natural (global) to the principal system.

The starting point is the heat diffusion equation for a single ply of a composite material. A single ply is an orthotropic material, which has by definition, at least two orthogonal planes of symmetry, where material properties are independent of direction. In such a material, thermal conductivity is not scalar but a tensor. In the coordinate system of the principal axes (where the number of nonzero elements of the tensor is minimized) coinciding with the axes parallel and perpendicular to the fibers, the heat diffusion equation for a single ply is expressed as follows:

$$k_{\parallel} \frac{\partial^2 T_s}{\partial x^2} + k_{\perp} \frac{\partial^2 T_s}{\partial y^2} + k_{\perp} \frac{\partial^2 T_s}{\partial z^2} - \rho C \frac{\partial T_s}{\partial t} = Q, \quad (1)$$

where k_{\parallel} (W/mK) and k_{\perp} (W/mK) are the thermal conductivity values parallel and vertically to the fibers, respectively. ρ (kg/m³) is the density, C (J/kg K) is the specific heat of the material, and Q (W/m³) is the periodically modulated heat source intensity,

$$Q = \frac{I_0}{2} \beta e^{-\beta z} e^{i\omega t} g(x, y), \quad (2)$$

where I_0 (W/m²) is the optical intensity, β (m⁻¹) is the optical absorption coefficient, ω (rad/s) is the excitation frequency, and $g(x, y)$ is dimensionless and quantifies the shape of the excitation in the x - y plane on the surface of the object at $z=0$. The shape of the source had Gaussian, line-focused Gaussian, or grating distribution (expanded Gaussian-line-focused Gaussian distribution can be used in practice when laser power is insufficient to have good signal; to eliminate the influence of the diffusion vertically to the axis of the line source, the resulting field is integrated along this direction—combined with a spatial square-wave filter), thus

$$g(x, y) = e^{-(x^2+y^2)/R^2} \quad \text{Gaussian} \quad (3a)$$

$$= e^{-[(x^2/R_x^2)+(y^2/R_y^2)]} \quad \text{Line-focused Gaussian} \quad (3b)$$

$$= \frac{1}{2} e^{-[(x^2/R_x^2)+(y^2/R_y^2)]} \times \left(1 + \operatorname{sgn} \left\{ \sin \left[\frac{2\pi(x-x_0)}{\lambda} \right] \right\} \right) \quad \text{Grating,} \quad (3c)$$

where R (m) is the radius of the Gaussian distribution, R_x (m) and R_y (m) are the axes of the asymmetric (elliptical) line-focused Gaussian distribution, λ (m) is the wavelength of the grating, and x_0 (m) is the position of the beam (maximum of the Gaussian distribution) with respect to the square-wave pattern. The three different distributions are depicted in Fig. 2.

If the orthogonal coordinate system xyz is rotated from the principal directions, the expression of the heat diffusion in a single ply [Eq. (1)] is changed. If we assume a rotation angle θ [Fig. 1(b)] of both x and y axes (x - y plane coincides with the plane of the composite laminate), the general expression for an orthotropic material becomes

$$k_{xx} \frac{\partial^2 T}{\partial x^2} + k_{yy} \frac{\partial^2 T}{\partial y^2} + k_{zz} \frac{\partial^2 T}{\partial z^2} + (k_{xy} + k_{yx}) \frac{\partial^2 T}{\partial x \partial y} = \rho C \frac{\partial T}{\partial t} + Q, \quad (4)$$

with

$$\begin{aligned} k_{xx} &= k_{\parallel} \cos^2 \theta + k_{\perp} \sin^2 \theta, \\ k_{xy} &= k_{yx} = (k_{\perp} - k_{\parallel}) \sin \theta \cos \theta, \\ k_{yy} &= k_{\perp} \cos^2 \theta + k_{\parallel} \sin^2 \theta, \quad k_{zz} = k_{\perp}. \end{aligned} \quad (5)$$

Assuming a harmonic time dependence of the solution, after applying a Fourier transform in the time domain and a two-dimensional (2D) Fourier transform in the spatial domain, the diffusion equation reduces to an ordinary second order differential equation with respect to the third spatial coordinate,

$$a \frac{\partial^2 \tilde{T}}{\partial z^2} + b \frac{\partial \tilde{T}}{\partial z} + cT = \frac{I_0}{2} \beta e^{-\beta z} \tilde{G}(f_x, f_y), \quad (6)$$

where

$$\tilde{T}(f_x, f_y, z) = \int \int_{-\infty}^{+\infty} T(x, y, z) e^{-2j\pi(f_x x + f_y y)} dx dy, \quad (7)$$

$$\tilde{G}(f_x, f_y) = \int \int_{-\infty}^{+\infty} g(x, y) e^{-2j\pi(f_x x + f_y y)} dx dy, \quad (8)$$

and

$$\begin{aligned} a &= k_{zz}, \quad b = 0, \\ c &= -4\pi^2 [k_{xx} f_x^2 + k_{yy} f_y^2 + 2k_{xy} f_x f_y] - j\omega \rho C, \end{aligned} \quad (9)$$

where f_x and f_y are the Fourier coordinates. The coefficients a , b , and c have a different influence on the formation of the temperature field. a is mainly related to the transfer of energy along z and b describes beam steering effects.⁴¹ Notice that, in the case of multilayered composites, b equals zero. c in-

dicates a preferential spreading of the spectrum, depending on the various conductivities, which result in a loss of field symmetry. The general solution of Eq. (6) consists of the solution of the homogeneous equation and the particular solution for the considered excitation. For a single layer, it can be written as

$$\begin{aligned} \tilde{T}(f_x, f_y, z, \omega) &= U(f_x, f_y, \omega) e^{m_1 z} + V(f_x, f_y, \omega) e^{m_2 z} \\ &\quad + F(f_x, f_y, z, \omega), \end{aligned} \quad (10)$$

where

$$F(f_x, f_y, z, \omega) = \frac{1}{2} \left(\frac{1}{a\beta^2 + c} \right) I_0 \beta e^{-\beta z} \tilde{G}(f_x, f_y), \quad (11)$$

and

$$\begin{aligned} m_{1,2} &= \pm \sqrt{-\frac{c}{a}} \\ &= \pm \sqrt{\frac{4\pi^2 [k_{xx} f_x^2 + k_{yy} f_y^2 + 2k_{xy} f_x f_y] + j\omega \rho C}{k_{zz}}}, \end{aligned} \quad (12)$$

where U and V (K) are coefficients, which are to be found from the boundary conditions, and $m_{1,2}$ (m^{-1}) represents the effective complex thermal wave number along the z axis. The real part of the inverse quantity $1/m_{1,2}$ represents the effective thermal diffusion length along the z axis.

MULTILAYER MODEL

Composite materials consist of a stack of thin layers (a single layer is called lamina) [Fig. 1(a)]. When a localized external heat source is applied to a composite sample, the thermal-wave field is formed according to the contribution of different layers. As will be shown in the following sections, the anisotropy of each of the material layers within the reach of thermal diffusion on the time scale of the modulation adds a unique feature to the thermal response at the surface. Our analytical solution for a multilayered model also allows us to describe delamination defects, via modified boundary conditions between the layers.

Each lamina composing the laminate is unidirectional, elastically, and thermally orthotropic, with its thermal conductivity given in global coordinates by Eq. (5). A schematic representation of the structure under investigation is depicted in Fig. 3. Every layer i is characterized by the thermal conductivity coefficient tensor \mathbf{k}_i and the scalar density ρ_i , the specific heat c_i , the absorption coefficient β_i , and the thickness l_i . It is assumed in our study that there is no reflection of light at the interfaces between layers and that all of the properties are constant within a layer. The harmonic power density in the i th layer is given by the Beer-Lambert law expressed as follows:

$$Q_i = \frac{I_0 \beta_i g(x, y)}{2} \exp[-\bar{\beta}_{i-1} + \beta_i(z + \bar{l}_{i-1})] \exp(j\omega t), \quad (13)$$

where

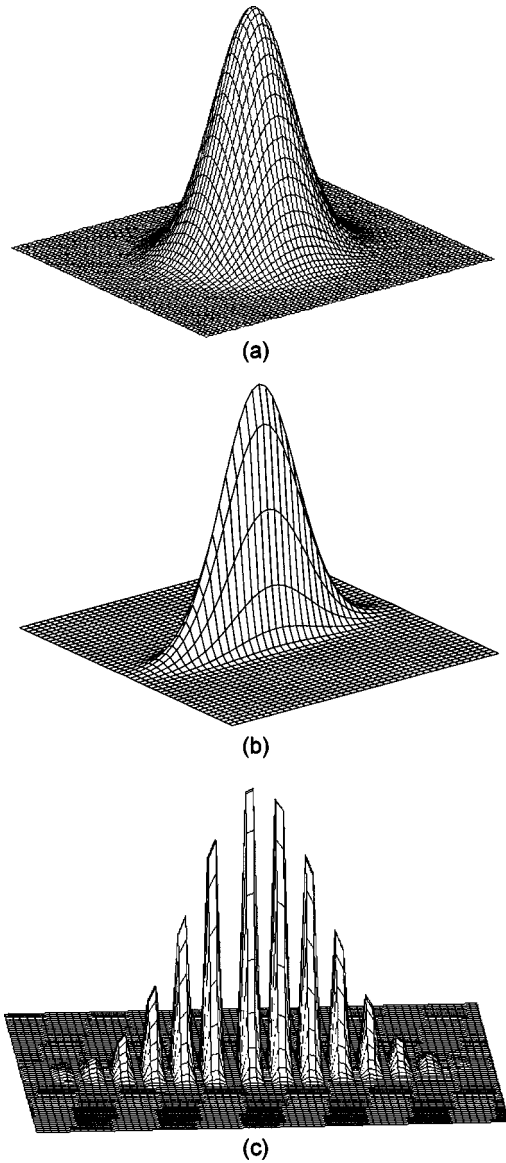


FIG. 2. (a) Gaussian, (b) line-focused Gaussian, and (c) grating heat source distribution.

$$\bar{\beta}_{i-1} = \sum_{n=1}^{i-1} \beta_n l_n \quad \text{and} \quad \bar{l}_{i-1} = \sum_{n=1}^{i-1} l_n.$$

The layers of the composite lie perpendicular to the z axis and the boundaries of the laminate are in contact with infinitely extended air. The equations can be solved in a straightforward way for a multilayered geometry to provide the thermal-wave field at any depth considering the continuity of temperatures and heat flows at the interfaces. For the choice of heat sources described in Eq. (10), the set of solutions for the system temperature profile can be formulated as follows (assuming that there are N layers including the two semi-infinite layers—of air or any other material—at the borders in the z direction):

$$\tilde{T}_0(f_x, f_y, z, \omega) = V_0(f_x, f_y, \omega) e^{-m_0 z},$$

$$\begin{aligned} \tilde{T}_1(f_x, f_y, z, \omega) &= U_1(f_x, f_y, \omega) e^{m_1 z} \\ &+ V_1(f_x, f_y, \omega) e^{-m_1 z} \\ &- F_1(f_x, f_y, z, \omega), \end{aligned}$$

$$\begin{aligned} \tilde{T}_2(f_x, f_y, z, \omega) &= U_2(f_x, f_y, \omega) e^{m_2(z+l_1)} \\ &+ V_2(f_x, f_y, \omega) e^{-m_2(z+l_1)} \\ &- F_2(f_x, f_y, z, \omega), \end{aligned}$$

...

$$\begin{aligned} \tilde{T}_i(f_x, f_y, z, \omega) &= U_i(f_x, f_y, \omega) e^{m_i(z+\bar{l}_{i-1})} \\ &+ V_i(f_x, f_y, \omega) e^{-m_i(z+\bar{l}_{i-1})} \\ &- F_i(f_x, f_y, z, \omega), \end{aligned}$$

...

$$\begin{aligned} \tilde{T}_{N-1}(f_x, f_y, z, \omega) &= U_{N-1}(f_x, f_y, \omega) e^{m_{N-1}(z+\bar{l}_{N-2})} \\ &+ V_{N-1}(f_x, f_y, \omega) e^{-m_{N-1}(z+\bar{l}_{N-2})} \\ &- F_{N-1}(f_x, f_y, z, \omega), \end{aligned}$$

$$\tilde{T}_N(f_x, f_y, z, \omega) = U_N(f_x, f_y, \omega) e^{m_N(z+\bar{l}_{N-1})} - F_N(f_x, f_y, z, \omega), \tag{14}$$

where

$$\begin{aligned} \tilde{F}_i(f_x, f_y, z, \omega) &= \frac{\tilde{Q}_i(f_x, f_y, z, \omega)}{a_i \beta_i^2 + c_i} \\ &= \frac{\tilde{Q}_i(f_x, f_y, z, \omega)}{k_{zz}^i \beta_i^2 - 4\pi^2 [k_{xx}^i f_x^2 + k_{yy}^i f_y^2 + 2k_{xy}^i f_x f_y] - j\omega \rho_i C_i}. \end{aligned} \tag{15}$$

Continuity of temperature and normal heat flux at the interfaces is equivalently valid in the temporally and spatially Fourier-transformed solution $\tilde{T}(f_x, f_y, z, \omega)$, just as in the Cartesian formulation $T(x, y, z, \omega)$.⁴² Applying these boundary conditions yields a set of $2N$ linear equations of the $2N$ unknown coefficients, $U = [U_1, U_2, \dots, U_N]$ and $V = [V_0, V_1, \dots, V_{N-1}]$,

$$\hat{A} \cdot \hat{U} = \hat{F}, \tag{16}$$

which can be solved very fast for a reasonable number of layers. The three-dimensional Fourier-transformed temperature field can thus be determined for every value of f_x , f_y , z , and ω . The band diagonal matrix \hat{A} and the vectors \hat{U} and \hat{F} of Eq. (16) are given by

$$\hat{A} = \begin{bmatrix} 1 & -e^{-m_{\nu-1}l_{\nu-1}} & -e^{m_{\nu-1}l_{\nu-1}} & \dots & 0 & 0 & 0 & 0 & \dots & 0 & 0 & 0 & 0 & 0 \\ b_{\nu} & -e^{-m_{\nu-1}l_{\nu-1}} & e^{m_{\nu-1}l_{\nu-1}} & \dots & 0 & 0 & 0 & 0 & \dots & 0 & 0 & 0 & 0 & 0 \\ \dots & \dots \\ 0 & 0 & 0 & \dots & 1 & 1 & -e^{-m_{i-1}l_{i-1}} & -e^{m_{i-1}l_{i-1}} & \dots & 0 & 0 & 0 & 0 & 0 \\ 0 & 0 & 0 & \dots & b_i & -b_i & -e^{-m_{i-1}l_{i-1}} & e^{m_{i-1}l_{i-1}} & \dots & 0 & 0 & 0 & 0 & 0 \\ \dots & \dots \\ 0 & 0 & 0 & \dots & 0 & 0 & 0 & 0 & \dots & 1 & 1 & -e^{-m_1l_1} & -e^{m_1l_1} & 0 \\ 0 & 0 & 0 & \dots & 0 & 0 & 0 & 0 & \dots & b_2 & -b_2 & -e^{-m_1l_1} & e^{m_1l_1} & 0 \\ 0 & 0 & 0 & \dots & 0 & 0 & 0 & 0 & \dots & 0 & 0 & 1 & 1 & -1 \\ 0 & 0 & 0 & \dots & 0 & 0 & 0 & 0 & \dots & 0 & 0 & 1 & -1 & w \end{bmatrix},$$

$$\hat{U} = \begin{bmatrix} U_{\nu} \\ U_{\nu-1} \\ V_{\nu-1} \\ \dots \\ U_i \\ V_i \\ U_{i-1} \\ V_{i-1} \\ \dots \\ U_2 \\ V_2 \\ U_1 \\ V_1 \\ \Phi_0 \end{bmatrix},$$

$$\hat{F} = \begin{bmatrix} F_{\nu}(-\bar{l}_{\nu-1}) - F_{\nu-1}(-\bar{l}_{\nu-1}) \\ (\beta_{\nu}k_{\nu}/m_{\nu-1}k_{\nu-1})F_{\nu}(-\bar{l}_{\nu-1}) - (\beta_{\nu-1}/m_{\nu-1})F_{\nu-1}(-\bar{l}_{\nu-1}) \\ \dots \\ F_i(-\bar{l}_{i-1}) - F_{i-1}(-\bar{l}_{i-1}) \\ (\beta_i k_i/m_{i-1}k_{i-1})F_i(-\bar{l}_{i-1}) - (\beta_{i-1}/m_{i-1})F_{i-1}(-\bar{l}_{i-1}) \\ \dots \\ F_2(-l_1) - F_1(-l_1) \\ (\beta_2 k_2/m_1 k_1)F_2(-l_1) - (\beta_1/m_1)F_1(-l_1) \\ F_1(0) \\ (\beta_1/m_1)F_1(0) \end{bmatrix},$$

$$b_i = k_i m_i / k_{i-1} m_{i-1}, \quad w = k_0 m_0 / k_1 m_1, \quad (17)$$

where the parameters b_i play the role of thermal-wave interfacial coupling coefficients and $w=1/b_1$. These coefficients quantify the degree of thermal inhomogeneity across the boundary planes (ratio of thermal impedances)⁴³⁻⁴⁵ and reduce to an effusivity ratio in the one-dimensional case, where the thermal effusivity ε (J m⁻² K⁻¹ s^{-1/2}) is defined as follows:

$$\varepsilon = \sqrt{k\rho C}. \quad (18)$$

To find the time harmonic solution in the Cartesian coordinates, one has to apply the inverse Fourier transform,

$$T(x,y,z,\omega) = \int \int_{-\infty}^{+\infty} \tilde{T}(f_x, f_y, z, \omega) e^{2j\pi(f_x x + f_y y)} df_x df_y. \quad (19)$$

The most convenient way to evaluate Eq. (19), is by applying FFT,³⁹ which is much faster than numerical integration.³⁶ Some possible problems with FFT are discussed in Ref. 39, but provided a laterally wide enough integration range and sufficiently fine discretization, we did not encounter problems.

THEORETICAL SIMULATIONS FOR POINT SOURCE EXCITATION

Structural design with composite materials is based on the lay-up (stacking) of differently oriented layers (of unidirectional long fibers) composing a laminate. Optimizing the stacking sequence, one can tailor the global mechanical/thermal properties and fulfill certain technical specifications. It is interesting in this framework to gain some insight on the formation of the thermal-wave field under the influence of the stacking sequence of the composite. Although not demonstrated here, preliminary work³⁹ has shown that the amplitude and especially the phase of the temperature distribution can be used to determine the (sometimes unknown) stacking sequence. Inverse methods and neural networks can be used to find the underlying fiber orientations from the surface response.

In the following analysis, we demonstrate how the temperature amplitude and phase distribution changes with frequency as a result of deeper penetration. Two different composite lay-ups were chosen to serve this goal. The first one is a semi-infinite composite with the fibers of the surface layer cross oriented to the bulk material $[0^\circ/90^\circ]_\infty$ and the second is the classical quasi-isotropic laminate $[0^\circ/\pm 45^\circ/90^\circ]_S$.^{46,47} The excitation source in these simulations represents a tightly focused Gaussian laser beam [Fig. 2(a)], described by Eq. (3), with a radius $R=100 \mu\text{m}$ in order to allow the visualization of the anisotropic three-dimensional (3D) effects. All simulations are conducted for unit intensity

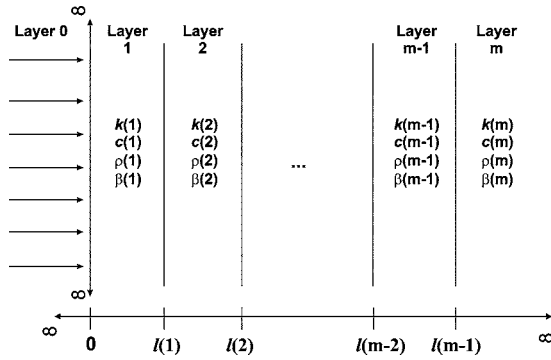


FIG. 3. Schematic representation of the multilayered model of a composite laminate.

$I_0=1 \text{ (W/m}^2\text{)}$. All the material properties used are given in Table I.^{35,48} The fibers of the 0° layers of the surface are supposed to be aligned along the vertical direction in the figures.

For both laminates considered, the results of the phase distribution shown in Figs. 4 and 5 evoke the following points.

- When the frequency is high, the thermal-wave field is dominated by the geometrical shape of the excitation source. The thermal diffusion length is too short at all directions to make any thermal anisotropy visible and the field at the surface appears to have a concentric circular form (i.e., a planar projection of the Gaussian source). More generally, the appearance of the anisotropy depends on the ratio of the source radius with respect to the effective thermal diffusion length for a particular frequency.
- As the frequency decreases, the field starts becoming elliptical under the influence of the thermal anisotropy. The eccentricity of the elliptical isothermals is increased all along with decreasing frequency when close to the source. The visibility of the preferential thermal diffusion along the fibers is gradually enhanced and the isothermals develop to concentric ellipses.
- When the frequency is low enough allowing the thermal wave to reach the second layer, with the orientation of the fibers at either 90° or 45° , then the concentric ellipses start deforming. In the first case (Fig. 4), the properties of the bulk material contribute so that the axes of the thermal diffusion ellipse are gradually

TABLE I. Material properties and geometrical parameters used for the simulations of the three-dimensional thermal-wave field in a fiber reinforced composite material.

Material properties	Source parameters	Geometry
$k_{ }=10.23 \text{ W/m}^2, k_{\perp}=0.56 \text{ W/m}^2$	$R=100 \text{ }\mu\text{m}$	$l_f=125 \text{ }\mu\text{m}$
$C=793 \text{ J/kg K}$	$I_0=1 \text{ W/m}^2$	
$\rho=1550 \text{ kg/m}^3$		
$\beta=10^9 \text{ m}^{-1}$		
$k_{\text{air}}=0.0258 \text{ W/m}^2$		
$C_{\text{air}}=1003 \text{ J/kg K}$		
$\rho_{\text{air}}=1.29 \text{ kg/m}^3$		

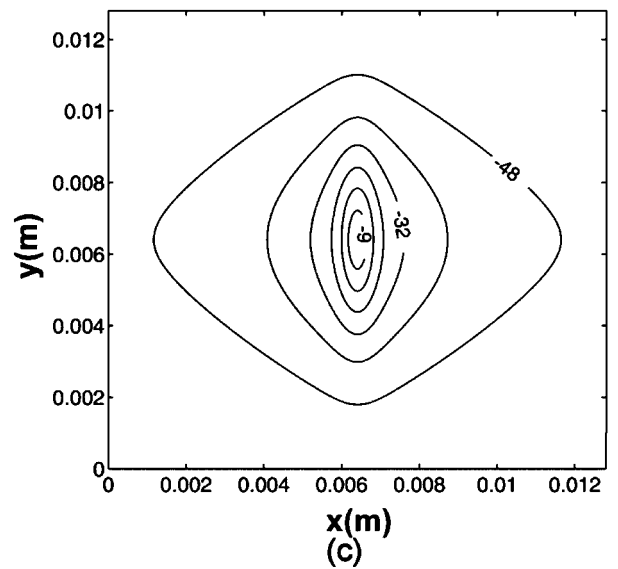
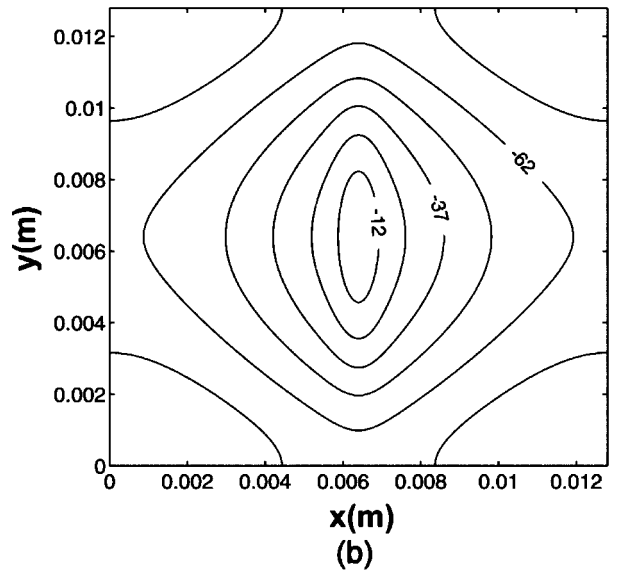
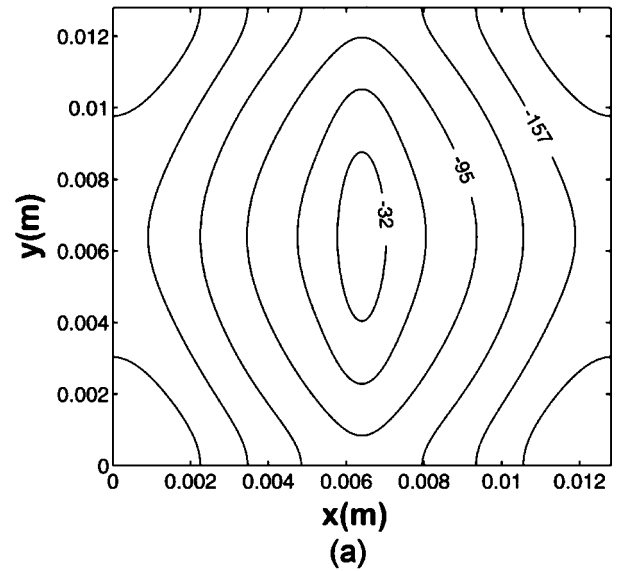


FIG. 4. Temperature phase maps at the surface of a ply ($125 \text{ }\mu\text{m}$) cross oriented to a semi-infinite bulk material ($0^\circ/90^\circ$), which is periodically heated with a Gaussian excitation source ($R=100 \text{ }\mu\text{m}$) at (a) 1, (b) 0.1, and (c) 0.01 Hz. The material properties are given in Table I.

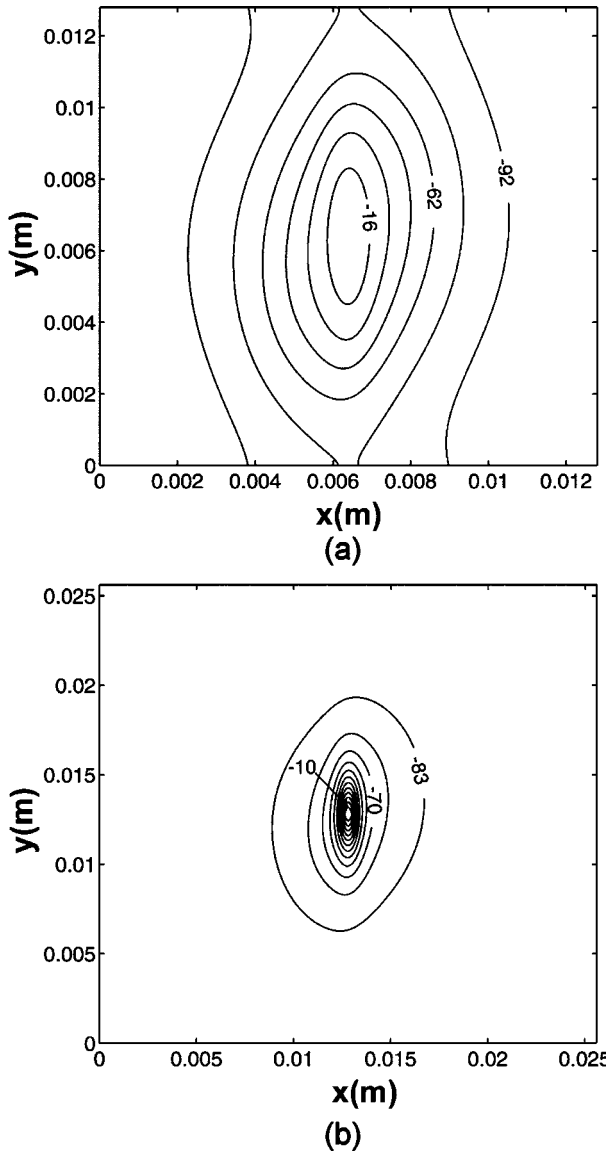


FIG. 5. Temperature phase contour maps at the surface of a quasi-isotropic composite material ($0^\circ/\pm 45^\circ/90^\circ$)_s, which is periodically heated with a Gaussian excitation source ($R=100\ \mu\text{m}$) at (a) 0.1 and (b) 0.005 Hz. The material properties are given in Table I.

inverted far from the source. In the second case (Fig. 5), the ellipse is rotated and compressed under the influence of the different fiber orientations and when the thermal diffusion length is longer than the thickness of the entire quasi-isotropic laminate, the field becomes approximately circular just like an isotropic material. The latter effect demonstrates that a quasi-isotropic laminate is macroscopically thermally isotropic.

- Far away from the source (several thermal diffusion lengths), the field is always configured according to the properties of the bulk material. The frequency only affects the scale of the effect. Consider, for instance, the first laminate (Fig. 4). When the frequency is low, the amplitude of the temperature oscillation of the inverted ellipse will be significant with respect to the maximum amplitude. When the frequency is very high, the ellipse will still be theoretically inverted but far away from the source where the amplitude of the

oscillation is so small that is probably experimentally not detectable.

- To make the previous point clearer in a phenomenological manner, we are led to the conclusion that the thermal-wave field has the same form of phase distribution no matter the excitation frequency. The characteristic morphology of the phase distribution depends only on the material properties. What the frequency affects is the scale of its representation. By observing Fig. 4 we see that increasing the frequency is as if one is zooming in to the center [Fig. 4(a) is a magnification of the central part of Fig. 4(c)]; notice that the dimensions of the area shown are the same for all the frequencies.

DETERMINATION OF THERMAL AND OPTICAL PROPERTIES

The simulations in the previous section illustrate that the thermal properties of the layers have a sophisticated influence on the thermal-wave field. Therefore, the inverse problem, extracting the thermal properties from the experimentally assessed thermal-wave field, is rather ill posed and complex. Moreover, the inverse problem is numerically very demanding in terms of computing time, because a number of iterations are needed to converge from an initial guess to the actual solution. This initial guess is therefore also crucial in the process.

The optothermal properties of a composite material are the thermal conductivities parallel and perpendicular to the fibers, k_{\parallel} and k_{\perp} , respectively, or k_1 , k_2 , and k_3 (in the case that the lateral thermal conductivity perpendicular to the fibers is not equal to the one across the thickness), the specific heat C , and the absorption coefficient β . The simplest configuration to determine these is to perform experiments on a simple, thermally thick (theoretically semi-infinite) unidirectional laminate. The 3D thermal-wave problem in the wave vector domain is then reduced into solving a simple 2×2 set of equations (described by Refs. 16 and 17 with index $m=1$). The surface solution in the Fourier space is then given by

$$\Theta_0(f_x, f_y, \omega) = \frac{I_0}{2} \left(\frac{\beta}{\beta + m_1} \right) \left(\frac{1}{k_{\text{air}} m_0 + k_{\perp} m_1} \right) \tilde{G}(f_x, f_y), \quad (20)$$

where β (m^{-1}) is the absorption coefficient of the composite and m_0 and m_1 (m^{-1}) are the effective thermal wave numbers in the air and the semi-infinite composite, respectively, given by

$$m_0 = \sqrt{4\pi^2(f_x + f_y)^2 + \frac{j\omega}{\alpha_{\text{air}}}}, \quad (21)$$

with

$$\alpha_{\text{air}} = \frac{k_{\text{air}}}{\rho_{\text{air}} C_{\text{air}}} \quad (\text{m}^2/\text{s}), \quad (22)$$

being the so-called thermal diffusivity, and

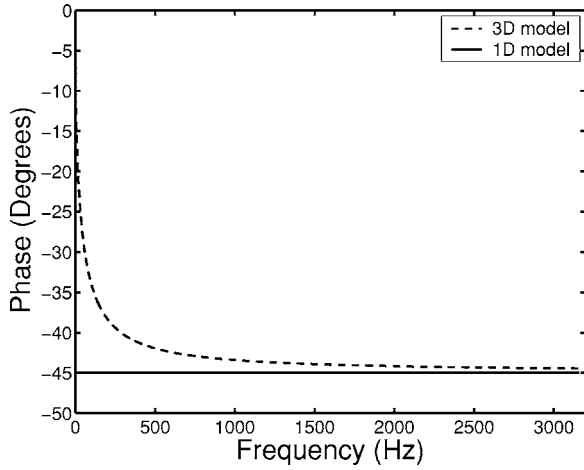


FIG. 6. The phase at the center of the Gaussian excitation with $R = 100 \mu\text{m}$ approaches that of uniform heating (-45°) as the frequency increases. The material is a semi-infinite solid with properties $k_{\parallel}=k_{\perp} = 1 \text{ W/mK}$, $C=800 \text{ J/kg K}$, $\rho=1550 \text{ kg/m}^3$, and $\beta=10^9 \text{ m}^{-1}$ in contact with air (properties given in Table I).

$$m_1 = \sqrt{\frac{4\pi^2(k_{\parallel}f_x^2 + k_{\perp}f_y^2) + j\omega\rho C}{k_{\perp}}}. \quad (23)$$

To solve this problem in practice, we have to define an area large enough to describe the thermal-wave field (the temperature amplitude at the edges of the area must be negligible) and avoid thus aliasing. Then the area is discretized densely enough to find convergence to the desired level of accuracy.

Before proceeding to the fitting process for the determination of the properties, we conducted a parametric study in order to analyze the influence of each property to the temperature field. The excitation frequency was set at 0.5 Hz and the Gaussian was tightly focused at $R=100 \mu\text{m}$ so that the 3D effects are emphasized [Fig. 6]. Unless otherwise specified, the conductivities along and perpendicular to the fibers are $k_{\parallel}=k_{\perp}=1 \text{ W/mK}$, the specific heat $C=800 \text{ J/kg K}$, and the density $\rho=1550 \text{ kg/m}^3$. The study was conducted both for highly (carbon fiber reinforcement $\beta=10^9 \text{ m}^{-1}$ approximately) and low (glass fiber reinforcement $\beta=10^2 \text{ m}^{-1}$ approximately) absorptive unidirectional semi-infinite composites in contact with air (properties given in Table I). The results are presented in terms of normalized amplitude and phase along the fibers and through the center of the Gaussian.

In highly absorptive composites, the ratio k_{\parallel}/k_{\perp} affects both the normalized amplitude and the phase of the temperature field (Fig. 7). With increasing ratio, both peaks become obtuse along the fibers due to the higher thermal diffusion. One can readily notice from Eq. (22) that the thermal diffusivity is proportional to the thermal conductivity. Regarding the normalized amplitude, the effect is stronger at high thermal conductivities with much more apparent change in the distribution. On the other hand, for low thermal conductivities (below the thick solid line representing the distribution for the reference property values), it converges to a certain distribution as the thermal diffusion length on one direction becomes shorter than the radius of the Gaussian excitation.

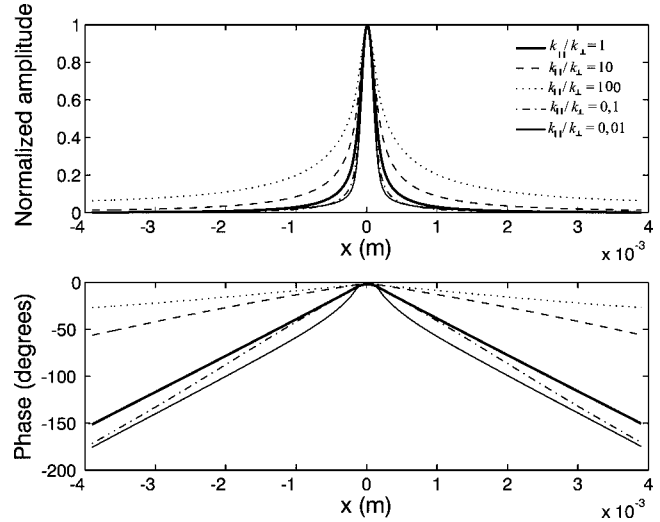


FIG. 7. Normalized amplitude and phase of temperature along the fibers and through the center of the Gaussian excitation heat source ($R=100 \mu\text{m}$) as a function of the ratio k_{\parallel}/k_{\perp} . The material is semi-infinite unidirectional composite with $C=800 \text{ J/kg K}$, $\rho=1550 \text{ kg/m}^3$, and $\beta=10^9 \text{ m}^{-1}$ in contact with air (Table I).

The significance of the geometry of the excitation at low conductivities is more profound in the phase distribution. For all the simulations except the last one (thin solid line), the phase is linearly decreased with distance from the center of the source but for that lowest ratio, there is a plateau indicating the transition. As shown in Fig. 8 and formulated in Eq. (22), the specific heat has the inverse effect on the thermal diffusion compared to the one of the conductivity with the normalized amplitude not affected for the range considered.

In composites with low absorption coefficient, the optical penetration has a strong influence on the formation of the thermal-wave field. For high thermal conductivities, the normalized amplitude similarly increases with distance but to a

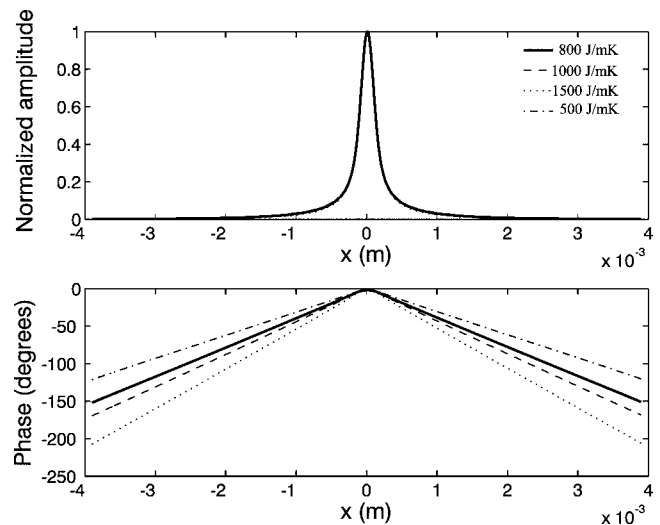


FIG. 8. Normalized amplitude and phase of temperature along the fibers and through the center of the Gaussian excitation heat source ($R=100 \mu\text{m}$) as a function of C . The material is semi-infinite unidirectional composite with $k_{\parallel}=k_{\perp}=1 \text{ W/mK}$, $\rho=1550 \text{ kg/m}^3$, and $\beta=10^9 \text{ m}^{-1}$ in contact with air (Table I).

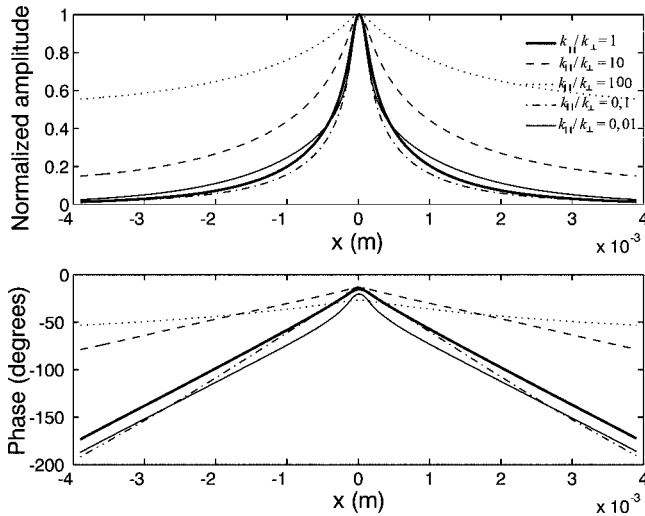


FIG. 9. Normalized amplitude and phase of temperature along the fibers and through the center of the Gaussian excitation heat source ($R=100\ \mu\text{m}$) as a function of the ratio k_{\parallel}/k_{\perp} . The material is semi-infinite unidirectional composite with $C=800\ \text{J/kg K}$, $\rho=1550\ \text{kg/m}^3$, and $\beta=10^2\ \text{m}^{-1}$ in contact with air (Table I).

much higher level (Fig. 9). As the thermal-diffusion length becomes shorter for lower thermal conductivities, thermal diffusion becomes less important than optical penetration in the formation of the thermal-wave field (thin solid line). The phase is also clearly much more affected with a change of the offset at the center of the excitation. The plateau is not present because of the optical penetration, but a similar effect is also apparent with a turning point in the linear pattern of phase decrease (thin solid line) and the subsequent intersection of the neighboring curves. Comparing Figs. 8 and 10, the specific heat value is rather more effective for low absorption regarding the normalized amplitude. The angle of the phase distribution in the same figures, on the other hand, is slightly sharper and displaced for lower absorption coeffi-

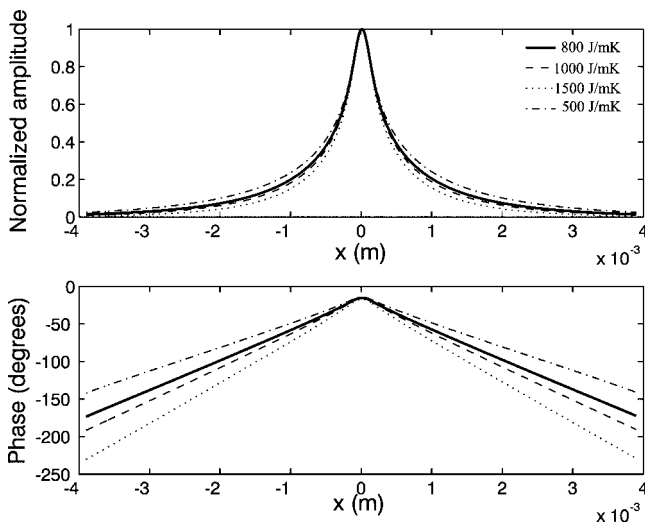


FIG. 10. Normalized amplitude and phase of temperature along the fibers and through the center of the Gaussian excitation heat source ($R=100\ \mu\text{m}$) as a function of C . The material is semi-infinite unidirectional composite with $k_{\parallel}=k_{\perp}=1\ \text{W/mK}$, $\rho=1550\ \text{kg/m}^3$, and $\beta=10^2\ \text{m}^{-1}$ in contact with air (Table I).

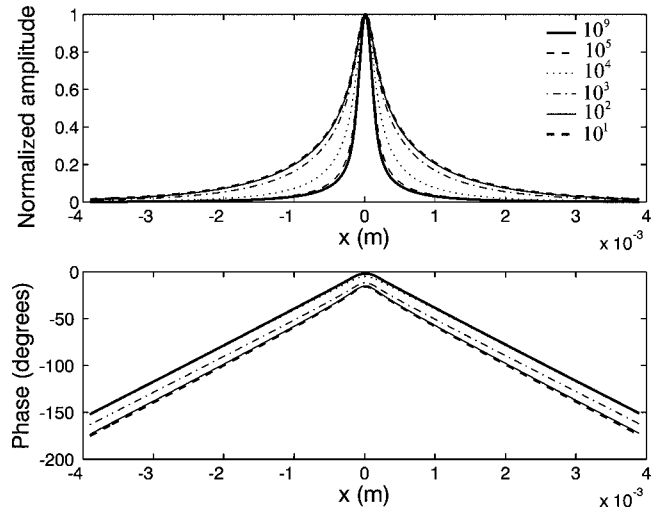


FIG. 11. Normalized amplitude and phase of temperature along the fibers and through the center of the Gaussian excitation heat source ($R=100\ \mu\text{m}$) as a function of β . The material is semi-infinite unidirectional composite with $k_{\parallel}=k_{\perp}=1\ \text{W/mK}$, $C=800\ \text{J/kg K}$, and $\rho=1550\ \text{kg/m}^3$ in contact with air (Table I).

cient values. This is also apparent in Fig. 11 where the pure effect of the absorption coefficient on the thermal-wave field in an isotropic ($k_{\parallel}=k_{\perp}$) material is shown.

From the previous analysis for focused excitation it is evident that solving the inverse problem has a problem of ill posedness because different parameters have similar effects on the signal. *A priori* information on some parameters thus has to be used as much as possible. In the following, we illustrate that also by using other source geometries, the influence of some parameters can be canceled, and thus the ill posedness of the problem for other parameters of interest can be lifted.

The first geometry is a simple Gaussian line source described by Eq. (3b) and shown in Fig. 2(b) applied along and perpendicular to the fibers. In this case, the diffusion along one axis in the plane is eliminated and the field can be described in two dimensions. This means that f_x and f_y in Eqs. (20)–(23) are alternately zero and, respectively, k_{\parallel} or k_{\perp} are not involved in the solution. The properties are then found by fitting the entire thermal-wave field along and perpendicular to the fibers for one or more excitation frequencies, preferably low enough to have adequate diffusion with respect to the line source width. Since the field is given along one dimension at the surface, this means a considerable reduction of the computation time. Moreover, the requirement for large memory in the case of matrix operations is eliminated.

The second geometry is similar in eliminating one of the plane conductivities, but the fitting procedure is simplified providing less uncertainty about the validity of our measurement. In practice, this geometry is achieved by expanding a Gaussian laser beam and sending it through a square-wave pattern, which is imaged by a lens onto the sample surface. The pattern has a wavelength λ as described by Eq. (3c) and shown in Fig. 2(c). The resulting photothermal field is shown in Figs. 12 and 13. The analytical solution in the simple case when uniform illumination combined with a grating, which is a sinusoidal spatial filter is shown to be given by

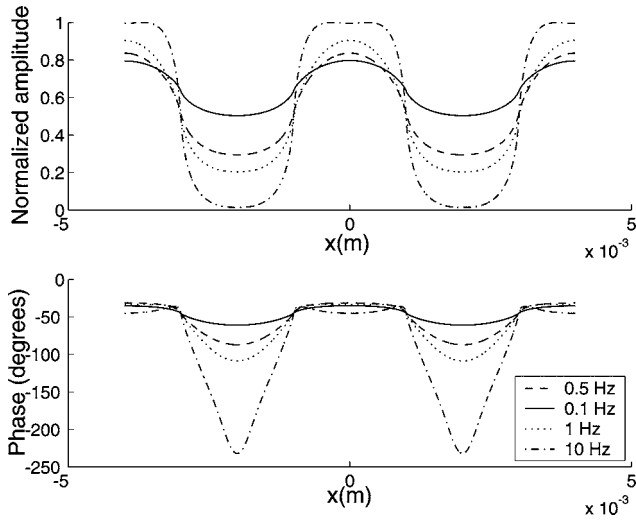


FIG. 12. Normalized amplitude and phase modulation of temperature perpendicularly to the grating bands ($\lambda=4\text{mm}$) and the fibers as a function of frequency. The material is semi-infinite unidirectional composite with $k_{\perp}=1\text{ W/mK}$, $C=800\text{ J/kg K}$, and $\rho=1550\text{ kg/m}^3$ in contact with air (Table I).

$$\Theta_G(f_x, \omega) = \frac{I_0}{2} \left(\frac{\beta}{\beta + m_1} \right) \left(\frac{1}{k_{\text{air}} m_0 + k_{\perp} m_1} \right) \times \left\{ \frac{j}{2} \left[\delta \left(f_x + \frac{1}{\lambda} \right) - \delta \left(f_x - \frac{1}{\lambda} \right) \right] \right\}, \quad (24)$$

where δ is the Dirac function and m_0 and m_1 (m^{-1}) are given in this case by

$$m_0 = \sqrt{4\pi^2 f_x + \frac{j\omega}{\alpha_{\text{air}}}}, \quad (25)$$

and

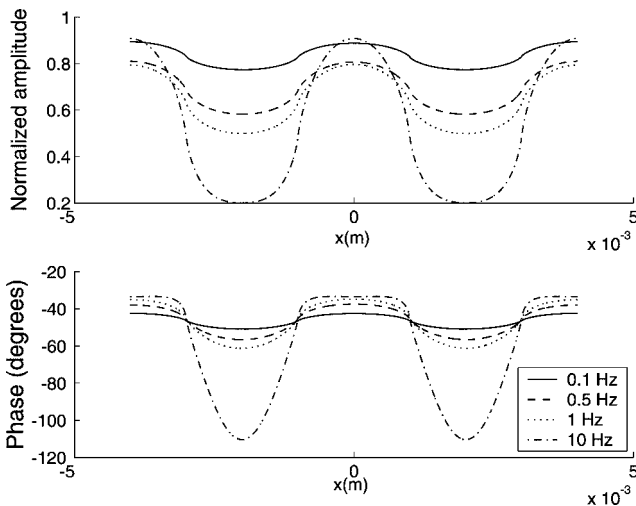


FIG. 13. Normalized amplitude and phase modulation of temperature perpendicularly to the grating bands ($\lambda=4\text{ mm}$) and parallel to the fibers as a function of frequency. The material is semi-infinite unidirectional composite with $k_{\parallel}=10\text{ W/mK}$, $k_{\perp}=1\text{ W/mK}$, $C=800\text{ J/kg K}$, and $\rho=1550\text{ kg/m}^3$ in contact with air (Table I).

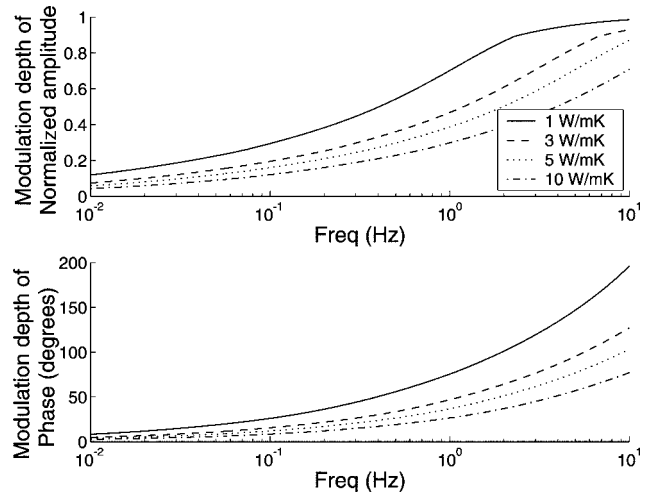


FIG. 14. Modulation amplitude of the normalized amplitude and phase of temperature as a function of frequency for different k_{\parallel} values. The first value $k_{\parallel}=1\text{ W/mK}$ corresponds to an isotropic material or the modulation perpendicularly to the fibers. The grating has $\lambda=4\text{ mm}$ and the material is semi-infinite unidirectional composite with $k_{\perp}=1\text{ W/mK}$, $C=800\text{ J/kg K}$, $\beta=10^9\text{ m}^{-1}$, and $\rho=1550\text{ kg/m}^3$ in contact with air (Table I).

$$m_1 = \sqrt{\frac{4k_{\parallel}\pi^2 f_x^2 + j\omega\rho C}{k_{\perp}}} \text{ or } \sqrt{\frac{4k_{\perp}\pi^2 f_x^2 + j\omega\rho C}{k_{\perp}}}, \quad (26)$$

depending whether the filter is positioned vertically or parallel to the fibers, respectively. The inverse Fourier transform of Eq. (24) gives the resulting temperature oscillation in space. The modulation depth of the temperature amplitude and phase can be easily determined from the absolute difference of the extremes of the modulation.

The measurement is no more bound to the excitation geometry (radius of the source or line width) and the previously fitted field is reduced to fitting two values, the amplitude of the field's normalized amplitude and phase modulation. The only *a priori* condition is that the excitation frequency has to be low enough so that the thermal waves from the opposite sides of an unheated zone due to the grating have effective wavelengths of the order of $\lambda/4$ so as to interfere with one another. As can be seen in Figs. 12 and 13 the modulation amplitudes are naturally reduced with lower frequency as a result of longer thermal diffusion lengths and increased washing out of periodical warm and cold zones. Apart from the numerical advantages already specified for the first approach of 2D analysis, the second fitting procedure is even faster as we do not fit the entire thermal-wave field along one dimension but only two values. Moreover, fitting is reduced to one graph depicting modulation amplitudes as a function of frequency (Figs. 14–16).

In the case that the laser power is insufficient to have good signal in practice, the beam can be line focused and then passed through the square-wave filter [Fig. 2(c)]. To eliminate the influence of the thermal diffusion vertically to the line source, one can integrate the resulting field in this direction.

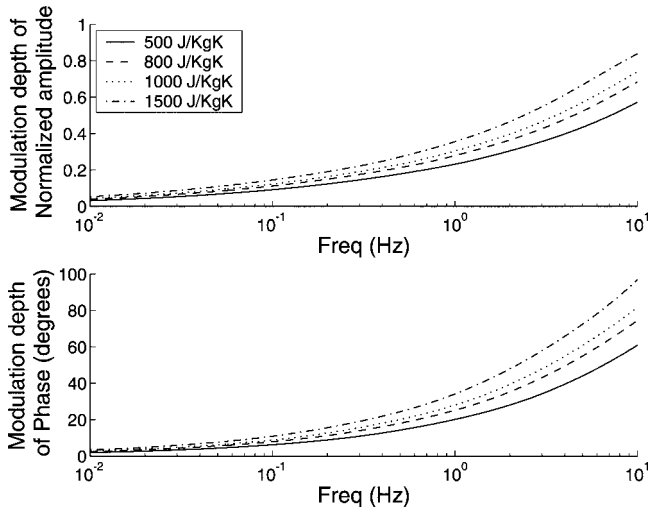


FIG. 15. Modulation amplitude of the normalized amplitude and phase of temperature as a function of frequency for different C values. The grating has $\lambda=4$ mm and the material is semi-infinite unidirectional composite with $k_{\parallel}=10$ W/mK, $k_{\perp}=1$ W/mK, $\beta=10^9$ m $^{-1}$, and $\rho=1550$ kg/m 3 in contact with air (Table I).

CONCLUSIONS AND DISCUSSION

In conclusion, the thermal-wave field in composite materials is much affected by the stacking sequence of the consisting layers. Theoretical simulations have demonstrated that in a quasi-isotropic sample the field alters from highly anisotropic to nearly isotropic, depending on the excitation frequency, which dictates the thermal diffusion length.

For the determination of the thermal properties, a method was proposed, which overcomes the ill posedness of the inverse problem. In contrast to the traditional approaches using focused or line-focused excitation, where several problems arise from this ill posedness, one can more accurately obtain the properties by applying a spatial filter on a uniform illumination, which results in a spatially modulated thermal-wave field. Moreover, the fitting process of the scalar modu-

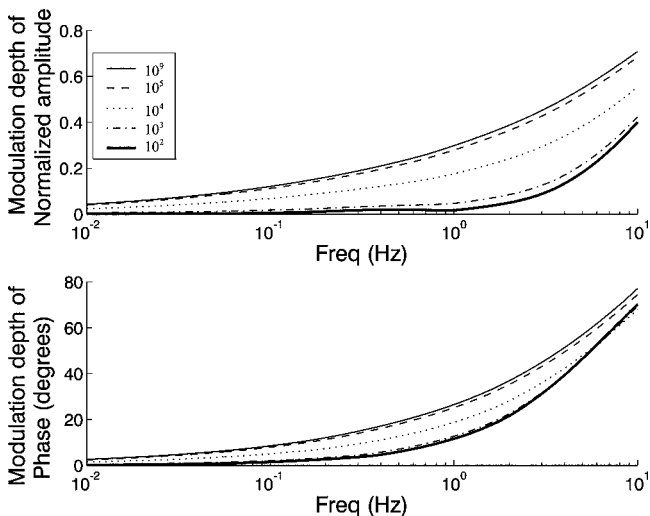


FIG. 16. Modulation amplitude of the normalized amplitude and phase of temperature as a function of frequency for different β values. The grating has $\lambda=4$ mm and the material is semi-infinite unidirectional composite with $k_{\parallel}=10$ W/mK, $k_{\perp}=1$ W/mK, $C=800$ J/kg K, and $\rho=1550$ kg/m 3 in contact with air (Table I).

lation depth of the amplitude and phase of the thermal-wave field is significantly faster than fitting the entire field, which was needed in the former methods.

Our theory is neglecting the possible presence of internal optical reflections, optical diffusion, and assumes constant thermal properties within a layer. In practice, e.g., with fiber composite materials, these conditions are not perfectly fulfilled, and not even well known. However, optical effects can be usually taken into account by fitting an effective optical absorption coefficient to the data, or they are smeared out due to the large number of fibers. Especially in the case of carbon fibers, the samples are quite opaque, and the effective optical penetration depth is typically quite small compared with the thermal diffusion length, thus its choice is not so crucial for the lateral thermal diffusion characteristics.

Experimental verification of the theoretical predictions, which is currently being conducted, proves the potential of this work, and it is going to be presented in due time.

- ¹H. S. Carslaw and J. C. Jaeger, *Conduction of Heat in Solids* (Oxford University Press, Oxford, 1959).
- ²J. M. Duhamel, *J. Ec. Polytech. (Paris)* **13**, 356 (1832).
- ³J. M. Duhamel, *J. Ec. Polytech. (Paris)* **19**, 155 (1848).
- ⁴G. Stokes, *Cambridge and Dublin Mathematical Journal* **6**, 215 (1851).
- ⁵V. J. Boussinesq, *Theorie analytique de la chaleur* (Gauthier-Villars, Paris, 1901).
- ⁶W. Voigt, *Lehrbuch der Krystallophysik* (BG Teubner, Leipzig, 1910).
- ⁷W. H. Giedt and D. R. HornBaker, *American Standard Report N.64-20727*, NASA CB-56137.
- ⁸K. J. Touryan, *AIAA J.* **2**, 124 (1964).
- ⁹B. T. Chao, *Appl. Sci. Res.* **12**, 134 (1962).
- ¹⁰J. Padovan, *AIAA J.* **10**, 60 (1972).
- ¹¹J. Padovan, *Int. J. Eng. Sci.* **13**, 247 (1973).
- ¹²D. Turkan and O. H. Tuna, *J. Pure Appl. Sci.* **8**, 69 (1975).
- ¹³Y. P. Chang, C. S. Kang, and D. J. Chen, *Int. J. Heat Mass Transfer* **16**, 1905 (1973).
- ¹⁴Y. P. Chang, *Int. J. Heat Mass Transfer* **20**, 1019 (1977).
- ¹⁵Y. P. Chang and C. H. Chou, *J. Heat Transfer* **99**, 41 (1977).
- ¹⁶Y. P. Chang and C. H. Chou, *J. Heat Transfer* **99**, 132 (1977).
- ¹⁷K. Katayama, *Int. J. Heat Mass Transfer* **4**, 137 (1975).
- ¹⁸C. R. Petts and H. K. Wickramasinghe, *Proc.-IEEE Ultrason. Symp.*, p. 832 (1981).
- ¹⁹M. H. Cobble, *Int. J. Heat Mass Transfer* **17**, 379 (1974).
- ²⁰W. Jackson and N. M. Amer, *J. Appl. Phys.* **51**, 3343 (1980).
- ²¹W. Jackson, N. M. Amer, A. Boccara, and D. Fournier, *Appl. Opt.* **20**, 1333 (1980).
- ²²M. A. Olmstead, N. M. Amer, S. Kohn, D. Fournier, and A. Boccara, *Appl. Opt.* **20**, 1333 (1983).
- ²³A. Ocariz, A. Sanchez-Lavega, and A. Salazar, *J. Phys. (Paris), Colloq.* **4**, 583 (1994).
- ²⁴A. Salazar, A. Sanchez-Lavega, A. Ocariz, J. Guitonny, J. C. Pandey, D. Fournier, and A. C. Boccara, *Appl. Phys. Lett.* **67**, 626 (1995).
- ²⁵A. Salazar, A. Sanchez-Lavega, A. Ocariz, J. Guitonny, J. C. Pandey, D. Fournier, and A. C. Boccara, *Appl. Phys. A: Mater. Sci. Process.* **79**, 3984 (1996).
- ²⁶A. Ocariz, A. Sanchez-Lavega, and A. Salazar, *Appl. Phys. A: Mater. Sci. Process.* **81**, 7552 (1997).
- ²⁷A. Ocariz, A. Sanchez-Lavega, and A. Salazar, *Appl. Phys. A: Mater. Sci. Process.* **81**, 7561 (1997).
- ²⁸A. Salazar, A. Sanchez-Lavega, and A. Ocariz, *Opt. Eng. (Bellingham)* **36**, 391 (1997).
- ²⁹A. Salazar and A. Sanchez-Lavega, *Int. J. Thermophys.* **19**, 625 (1998).
- ³⁰J. M. Terron, A. Salazar, and A. Sanchez-Lavega, *Appl. Phys. A: Mater. Sci. Process.* **89**, 5696 (2001).
- ³¹J. M. Terron, A. Salazar, and A. Sanchez-Lavega, *Appl. Phys. A: Mater. Sci. Process.* **91**, 1087 (2002).
- ³²A. Salazar, J. M. Terron, A. Sanchez-Lavega, and R. Cellorio, *Appl. Phys. Lett.* **80**, 1903 (2002).

- ³³A. Salazar, A. Sanchez-Lavega, and R. Cellorio, *Appl. Phys. A: Mater. Sci. Process.* **93**,4536 (2003).
- ³⁴F. Garrido and A. Salazar, *Appl. Phys. A: Mater. Sci. Process.* **95**, 140 (2004).
- ³⁵W. Lauriks, C. Desmet, C. Glorieux, and J. Thoen, *J. Mater. Res.* **8**, 3106 (1993).
- ³⁶J. C. Krapez, P. Cielo, X. Maldague, and L. A. Utracki, *Polym. Compos.* **8**, 396 (1987).
- ³⁷D. Wu, R. Steegmuller, W. Karpen, and G. Busse, *Rev. Prog. Quant. Nondestr. Eval.* **14**, 439 (1995).
- ³⁸W. Karpen, D. Wu, R. Steegmuller, and G. Busse, in *Quantitative Infrared Thermography, QIRT '94*, edited by D. Balageas, G. Busse, and G. M. Carlomagno (Européennes Thermique et Industrie, Paris, 1995), pp. 281–286.
- ³⁹W. Karpen, D. Wu, and G. Busse, *Res. Nondestruct. Eval.* **11**, 179 (1999).
- ⁴⁰P. Grosse and R. Wynands, *Appl. Phys. A: Solids Surf.* **48**, 59 (1989).
- ⁴¹M. Vaez Iravani and M. Nikoonahad, *J. Appl. Phys.* **62**, 4065 (1987).
- ⁴²C. Glorieux, J. Fizez, and J. Thoen, *J. Appl. Phys.* **73**, 684 (1993).
- ⁴³D. Almond and P. Patel, *Photothermal Science and Techniques* (Kluwer Academic, Dordrecht, 1996).
- ⁴⁴A. Mandelis, *Diffusion-Wave Fields* (Springer-Verlag, New York, 2001).
- ⁴⁵A. Mandelis, *Principles and Perspectives in Photothermal and Photoacoustic Phenomena* (Elsevier, New York, 1992).
- ⁴⁶D. Hull, *An Introduction to Composite Materials* (Cambridge University Press, Cambridge, 1981).
- ⁴⁷Laminate Orientation Code Devised by the Air Force Laboratory, Wright-Patterson Air Force Base, Ohio.
- ⁴⁸G. Kalogiannakis, D. Van Hemelrijck, and G. Van Assche, *J. Compos. Mater.* **38**, 163 (2004).